scientific reports

OPEN

Strong interfacial Dzyaloshinskii–Moriya induced in Co due to contact with NiO

M. Kowacz[1], P. Mazalski[2,3✉], I. Sveklo[2], M. Matczak[2], B. Anastaziak[1,4], U. Guzowska[2], A. K. Dhiman[2], E. Madej[3], A. Maziewski[2], P. Kuświk[1✉] & R. Gieniusz[2]

The magnetic properties of NiO/Co/Pt as a function of Co layer thickness were investigated by polar magneto-optical Kerr effect (PMOKE) (magnetometry and microscopy) and Brillouin Light Scattering (BLS) spectroscopy. PMOKE measurements revealed strong surface anisotropy (1.8 mJ/m^2) favoring perpendicular magnetic anisotropy and asymmetric domain wall propagation explained by anticlockwise chirality. BLS measurements show that this chirality is induced by strong interfacial Dzyaloshinskii–Moriya interaction (+ 2.0 pJ/m). This is one of the highest values reported so far for Co layers surrounded by different layers. The observed chirality is opposite to what has been found in Co/oxide interfaces. These results and data published earlier, indicate that the strength of interfacial Dzyaloshinskii–Moriya interaction increases with the amount of stoichiometric NiO. Therefore, this work shows that NiO is the source of the interfacial Dzyaloshinskii–Moriya interaction.

Currently, the interfacial Dzyaloshinskii–Moriya interaction (iDMI) is intensively studied in magnetic thin films. It is induced by inversion symmetry breaking and stabilizes chiral structures, including skyrmions. The investigation of iDMI in antiferromagnetic (AFM)/ferromagnetic (FM) systems with exchange bias (EB) coupling is of great importance because skyrmions can be stabilized at room temperature (RT) and zero magnetic field in FM films with perpendicular magnetic anisotropy (PMA) by interactions with AFM layers[1]. Moreover, since skyrmions can be created and destroyed with electric fields, insulating materials including oxides are needed as well[2]. The modification of electronic states around Fermi level at the interface between oxide and FM materials and its influence on magnetic properties are nontrivial, so different combinations of layer materials are studied both experimentally and numerically by first principles calculations[3–7]. Antiferromagnetic oxides (AFO) belongs to this group and can be ideal candidates towards the fulfillment of these requirements. However, only a few works so far have paid attention on how the AFO influences the iDMI in ferromagnets. Therefore we will focus on NiO, which strongly pins ferromagnetic spins by exchange bias coupling[8] and in stoichiometric form is an insulator (note that even single-crystal NiO may deviate from the proper stoichiometry Ni:O ratio (1:1) because of lattice defects (vacancies/interstitials)[9,10]).

Spin textures in exchange biased Au/Co/NiO systems show clockwise (CW) chirality; as inferred using asymmetric domain propagation[11] and magnetization reversal of micrometric-sized triangles[12]. In those systems, it was expected that the Au layer would not be the main source of interfacial DMI and the chirality would be supported only at the Co–CoO–NiO interface. Taking this into account the strength of iDMI (D_S) measured was not so high ($D_S = -1.1$ pJ/m) and could also be affected by the Co oxide layer that appeared at the interface between Co and NiO. On the other hand, the iDMI and EB coupling have also been investigated in Pt/Co/Ni$_x$O$_y$[13], where the concentration of the NiO phase was controlled by changing the Ar pressure during deposition. In that case, the maximum of $D_S = -1.25$ pJ/m was reached for 40% concentration of NiO in layers deposited by sputtering Ni$_x$O$_y$. Therefore, it is important to determine two facts about the nickel oxide layer obtained during pulsed laser deposition (PLD): (1) whether the concentration of stoichiometric NiO on it enhances iDMI; and, (2) which type of chirality does it support.

To investigate the iDMI, we used Brillouin light scattering (BLS) spectroscopy and the asymmetric domain propagation method based on polar magneto-optical Kerr effect (PMOKE) microscopy applying magnetic fields with in-plane and perpendicular components to the sample plane. We demonstrate that NiO(bottom)/Co/Pt(top) shows anticlockwise (ACW) chirality, which confirms earlier assumptions that the NiO layer is a strong source of

[1]Institute of Molecular Physics Polish Academy of Sciences, Poznań, Poland. [2]Faculty of Physics, University of Bialystok, Białystok, Poland. [3]Jerzy Haber Institute of Catalysis and Surface Chemistry, Polish Academy of Sciences, Kraków, Poland. [4]NanoBioMedical Centre, Adam Mickiewicz University in Poznan, Poznań, Poland. ✉email: piotrmaz@uwb.edu.pl; kuswik@ifmpan.poznan.pl
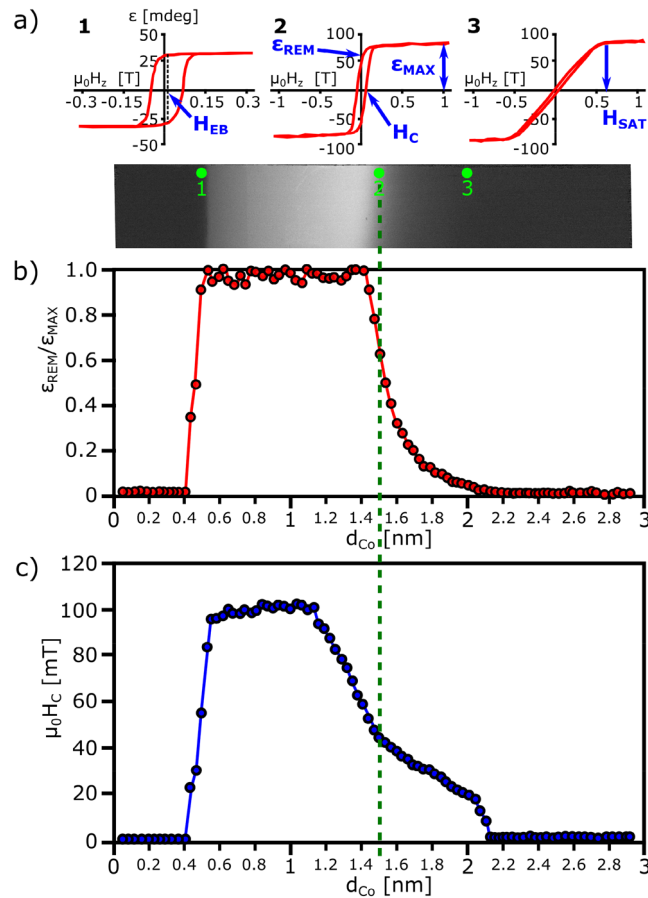
Figure 1. Results of PMOKE measurements. (**a**) Differential PMOKE microscope images registered in remanence after saturation with an out-of-plane magnetic field, where the bright area corresponds to the part of Co layer with PMA. This panel additionally shows the exemplary PMOKE hysteresis loops measured for $d_{Co} = 0.5, 1.5, 2$ nm (green dots 1 to 3, respectively). On that loops the definitions of characteristic parameters: remanence (ε_{REM}), ellipticity in maximal magnetic field (ε_{MAX}) and saturation field (H_{SAT}) and exchange bias field (H_{EB}) are given graphically; (**b,c**) d_{Co} dependencies of normalized Kerr signal $\varepsilon_{REM}/\varepsilon_{MAX}$ and, coercivity (H_C), respectively. The green dashed vertical line indicates the Co thickness for spin reorientation transition (see Fig. 2d).

iDMI and favors opposite chirality (in contrast to other non-antiferromagnetic oxides such as MgO and Al_2O_3). The investigation was performed on wedged samples, which enable measurements of iDMI in a wide range of Co thicknesses (d_{Co}). We found a large iDMI ($Ds = +2.0$ pJ/m), among the strongest reported on Co layers surrounded with different materials. Moreover, due to strong surface anisotropy contributions at the NiO/Co and Co/Pt interfaces (1.8 mJ/m^2), PMA holds up to $d_{Co} \cong 1.5$ nm.

Results

Magnetooptical studies. The magnetic ordering of the Co layer is determined from large field of view PMOKE microscope images (differential with respect to saturated state) registered in remanence after out-of-plane magnetic field saturation (Fig. 1a). The bright areas in this PMOKE image roughly correspond to the out-of-plane magnetization state; the dark areas, to the in-plane magnetization state of the thick Co layer, and to the non-ferromagnetic state of the thin Co layer. These data show that the PMA is observed in a wide d_{Co} range if Co is surrounded by NiO and Pt layers. To analyze this effect, we measured magnetization reversal along the Co wedge (as a function of d_{Co}) using PMOKE magnetometry. Figure 1a presents three exemplary hysteresis loops for $d_{Co} = 0.5, 1.5, 2$ nm. From these measurements, we were able to determine d_{Co} dependence of basic magnetic and magnetooptical parameters like coercive field H_C; ellipticity in remanence (ε_{REM}); and, at the maximum magnetic field (ε_{MAX}), saturation field (H_{SAT}) and exchange bias field (H_{EB}). These data confirm that the PMA is preserved in a wide d_{Co} range showing the rectangular shape of the hysteresis loop ($\varepsilon_{REM}/\varepsilon_{MAX} = 1$) up to the thickness for spin reorientation transition (SRT), $d_{SRT} \cong 1.5$ nm (Fig. 1b). Above d_{SRT}, the out-of-plane easy axis direction rotates to easy-plane. Since the deposition process was performed in an external out-of-plane magnetic field, the H_{EB} is detected with maximal value for $d_{Co} \sim 0.5$ nm and decreases for smaller Co thicknesses (not shown here). The presence of the EB coupling is also manifested by the large value of H_C, which is much higher than reported for non-oxide HM/Co/HM systems[14] (Fig. 1c). The reduction of H_C starts at lower d_{Co} than
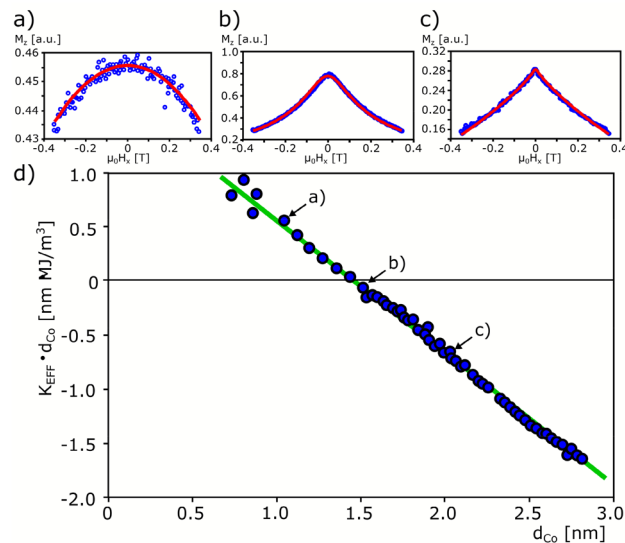
Figure 2. Magnetic anisotropy analysis: (**a–c**) exemplary PMOKE signal dependencies as function of in-plane field under a constant 0.15 T out-of-plane field. Red lines—fitting to the Stoner-Wohlfarth model, for selected $d_{Co} = 1, 1.5, 2$ nm, respectively. (**d**) $K_{1EFF}d_{Co}$ vs d_{Co}. Green line—A linear fit to $K_{1EFF}d_{Co} = K_V\,d_{Co} + 2K_S$ provides surface ($2K_S$) and volume (K_V) magnetic anisotropies. Points (**a–c**) in panel (**d**) correspond to d_{Co} in panels (**a–c**), respectively.

normalized ellipticity $\varepsilon_{REM}/\varepsilon_{MAX}$ due to strong influence of d_{Co} on domain propagation field near SRT[8]. While decreasing d_{Co} from SRT the magnetization reversal process is realized by domain nucleation mechanism—coercivity wall with large number of nucleation centers, then by domain wall propagation mechanism dominates (see Supplementary materials Fig. S1).

For the case of in-plane magnetization, the effective magnetic anisotropy field, H_{1EFF}, was determined as the saturation field H_{SAT} obtained from PMOKE magnetization reversal (see PMOKE loop 3 in Fig. 1a). The magnetic anisotropy constant K_{1EFF} was calculated according to the relation $K_{1EFF} = 1/2\mu_0 H_{1EFF}M_S$, where M_S is the saturation magnetization for bulk cobalt $\mu_0 M_s = 1.45$ T. In the case of out-of-plane magnetization and above d_{SRT}, where a weak in-plane magnetic anisotropy appears ($d_{Co} \leq 2$ nm), H_{1EFF} was determined by fitting the Stoner–Wohlfarth model[15] to the PMOKE signal measured as a function of the in-plane magnetic field under a constant out-of-plane magnetic field to ensure single domain state (see Fig. 2a–c).

Figure 2d shows the d_{Co} dependence of $K_{1EFF}\,d_{Co}$. We found that for thin Co layers ($d_{Co} \sim 0.6$ nm) the K_{1EFF} is much stronger than for other systems (e.g. Pt/Co/Pt, Pt/Co/Ir, Ir/Co/Pt) [14,16]. This strong PMA is associated with the presence of NiO and Pt as buffer and cover layers, respectively. The Pt layer supports the PMA owing to large spin–orbit coupling[17]; at the same time, hybridization between Co and O atoms at the NiO/Co interface can also be a source of PMA[18]. However, it was recently demonstrated that the AFM layer in the case of Co/NiO bilayer gives an additional contribution to magnetic anisotropy[19], which vanishes above Néel temperature of CoO/NiO layers[20]. Therefore, this coupling has a sufficiently strong surface contribution, which leads to the Co layer being magnetized perpendicularly to the sample plane in wider d_{Co} ranges than in other polycrystalline HM/Co/HM systems[19]. To determine the surface ($2K_S$) and volume (K_V) anisotropy contributions we used a linear fit to the $K_{1EFF}d_{Co}(d_{Co})$ dependence (Fig. 2d). From this fitting, we obtained $2K_S = 1.82 \pm 0.06$ mJ/m^2 and $K_V = -1.23 \pm 0.04$ MJ/m^3. Note that K_V includes the shape anisotropy contribution too. This high $2K_S$ value confirms that the surface contribution is a main source of PMA in NiO/Co/Pt. It should be emphasized that this value is also much higher than for similar NiO/Co/Au trilayers systems[11], Au/Co/NiO[19], Pt/Co/AlO$_x$[21], Ir/Co/AlO$_x$[22].

Recent results show that NiO in contact with the Co layer might be the source of iDMI[6]; therefore, we measured the domain propagation under a combination of in-plane H_x and out-of-plane H_z field pulses. iDMI has been confirmed as an origin of asymmetric domain wall propagation[23]. This effect occurs because the external in-plane magnetic field induces asymmetrical changes of the energy of Néel domain walls (N-DWs)[24]. Therefore, with the right combination of H_z and H_x, domain walls with core magnetizations pointing along and against H_x move at different speeds causing asymmetric growth of bubble domains. The studies were performed for $d_{Co} = 0.9$ nm where sufficiently large bubble-like domains appear. Because of high coercivity and magnetic anisotropy, it was necessary to use a strong H_z pulse for this experiment. In this experiment, we found such asymmetric domain growth in our samples (Fig. 3) confirming the presence of a strong iDMI. By analyzing the asymmetry of domain wall propagation for different directions of H_x and H_z fields, we determined the chirality of NiO/Co/Pt. Our data reveals that spin configuration in the N-DW has ACW chirality, which is related to a positive iDMI constant ($D_S > 0$). Note that D_S sign agrees with data presented in Ref.[13], which uses the reverse order of surrounding layers, namely Pt(bottom)/Co/Ni$_x$O$_y$(top), and found negative values of iDMI. For this system, it has also been shown that the magnitude of $|D_S|$ increases with larger concentrations of stoichiometric NiO in the nickel oxide layer. However, use of the sputtering technique for nickel oxide in Ar + O$_2$ atmosphere presented in Ref.[13] did not allow
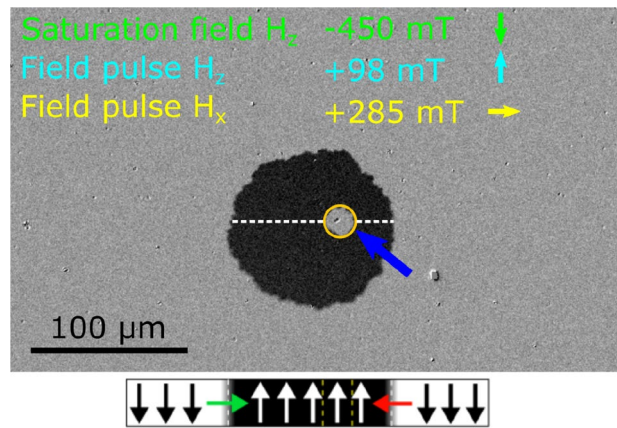
Figure 3. PMOKE difference image of the bubble domain growth with applied in-plane H_x and out-of-plane H_z fields for the buffer/NiO(10 nm)/Co(0.9 nm)/Pt(5 nm) system. The values and directions of applied fields are shown in the image. The yellow ring indicates the initial position of the initial bubble domain. Place below the image there is a scheme of the lateral magnetization profile along the dashed white line shown above. The N-DWs are marked by red and green arrows indicating anticlockwise chirality.
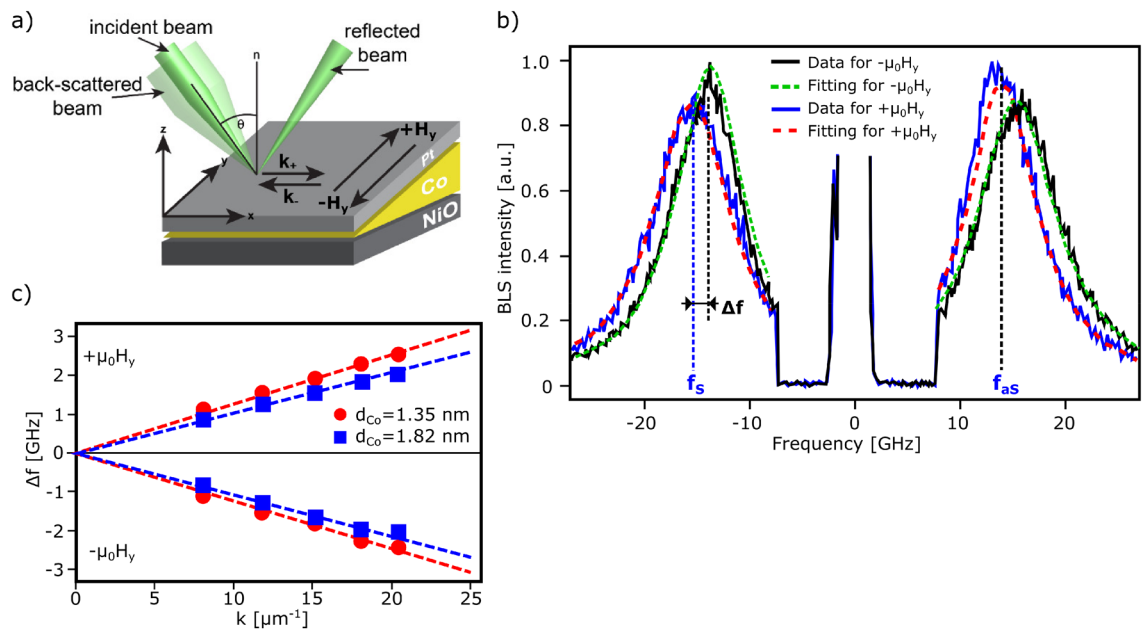
Figure 4. Results of BLS measurements. (**a**) BLS schematic for Damon-Eshbach configuration: magnetic field is applied in the sample plane along y; xz—plane of incidence, θ—incidence angle; studied SW wave vector k is along x; (**b**) BLS spectrum acquired for $k = 11.81\ \mu m^{-1}$, $\mu_0 H_y = -0.4$ T (black curve) and $\mu_0 H_y = +0.4$ T (blue curve) for $d_{Co} = 1.35$ nm with the definition of the characteristic parameters: the Stokes frequency f_S, the anti-Stokes frequency f_{aS}, frequency difference Δf; the dashed red (green) lines represent the peaks fittings to the positive (negative) in-plane field. (**c**) $\Delta f(k)$ dependence measured for positive ($+\mu_0 H_y$) and negative ($-\mu_0 H_y$) in-plane fields for $d_{Co} = 1.35$ nm (red dots) and 1.82 nm (blue squares); red (blue) dashed lines—linear fits passing through (0;0) for $d_{Co} = 1.35$ nm (1.82 nm). The error of the $\Delta f(k)$ is 0.05 GHz and 0.07 GHz for $d_{Co} = 1.35$ and 1.82 nm, respectively.

to obtain NiO concentrations larger than 40%. Despite this, a quite strong iDMI with a maximal value of $D_S \approx -1.2$ pJ/m was found. Based on those results, we expected that more stoichiometric NiO would further enhance the iDMI. Therefore, we grew NiO layer using PLD techniques in O_2 atmosphere reusing earlier parameters[11]. This allows us to check the influence of NiO on the iDMI strength with BLS measurements.

Brillouin light scattering studies. BLS measurements were performed in the Damon–Eshbach (DE) configuration (see a schematic of the measurement setup in Fig. 4a). Figure 4b shows exemplary BLS spectra for Co layer thicknesses, $d_{Co} = 1.35$ nm. The frequency difference between BLS peaks was measured for two opposite
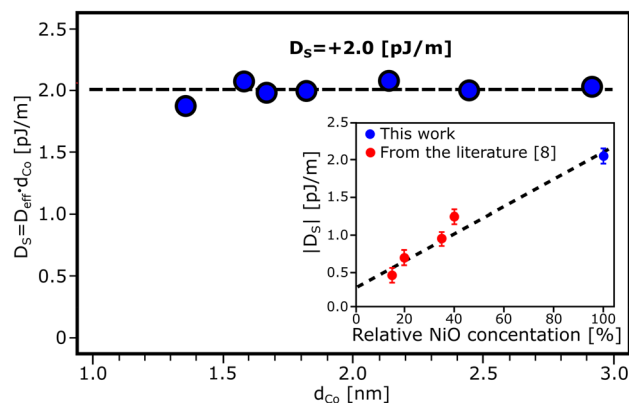
Figure 5. Magnitude of iDMI (D_S) as a function of cobalt thickness (d_{Co}) for NiO/Co/Pt. The inset shows D_s as a function of the relative concentration of NiO phase; for Pt/Co/Ni$_x$O$_y$ (data are taken from[13], red filled circle, negative D_s) and for NiO/Co/Pt (this work, blue filled circle positive Ds) samples, respectively. The dashed line is a linear fit.

directions of the applied in-plane magnetic field. By comparing curves for opposite field orientation, the difference Δf between frequency of Stokes (f_S) and anti-Stokes (f_{aS}) peaks can be obtained ($\Delta f = f_S - f_{aS}$)(see Fig. 4b).

These measurements were performed for different k values by changing the incident angle Θ to determine the effective iDMI constant ($D_{eff} \equiv D_S/d_{Co}$) from $\Delta f(k)$ relation[25–27]:

$$\Delta f(k) = 2\gamma D_{eff}k/\pi M_S \qquad (1)$$

where γ is the gyromagnetic ratio, M_s magnetization saturation of magnetic layer (for Co we used $\mu_0 M_S = 1.45$ T, $\gamma = 170$ GHz/T). Figure 4c shows examples of $\Delta f(k)$ dependencies for different Co thicknesses ($d_{Co} = 1.35$ and 1.82 nm) measured for positive and negative directions of the applied in-plane magnetic fields. From the analysis of the results shown in Fig. 4c we found this typical behavior for samples with iDMI: (i) the sign of the slope in $\Delta f(k)$ dependence reverses with the field direction; (ii) this slope (corresponds to the increase of D_{eff}) increases as d_{Co} decreases. Since the BLS measurements were performed along the Co wedge, the value of D_{eff} was determined for a wide d_{Co} range.

Figure 5 presents the dependence of the product $D_{eff} \cdot d_{Co}$ as a function of d_{Co}. The iDMI constant (D_s) can be determined since this value is independent of d_{Co} in the measured range. The value obtained, $D_S = +2.0$ pJ/m, is higher than those observed in similar systems (e.g. Au/Co/NiO trilayers where $D_S = -1.11$ pJ/m[8,12] and Pt/Co/Ni$_y$O$_x$ where $-0.5 < D_S < -1.2$ pJ/m depending on Ar pressure during deposition[13]). Note that, as the order of the cobalt layer covers is reversed[13], the sign of D_S changes too; therefore, the chirality set by NiO is the same. Moreover, considering the data from Ref.[13] and our data, we infer that the magnitude of the D_S increases together with the concentration of NiO phase. It should be mentioned that the relative NiO concentration in[13] was obtained as a ratio of 529.9 eV to 532.6 eV XPS peaks of O 1 s spectra, whereas in[11] 100% NiO concentration was deduced from Ni 2p spectra. The composition of NiO layer deposited by PLD was also evaluated from the reference sample (50 nm of NiO) described in the Supplementary Materials (Fig. S2). This allows us to to show that there is linear dependence of D_S on stoichiometric NiO phase concentration (inset in Fig. 5). Note that the deposition process of NiO was much different for both systems (Ni$_x$O$_y$ was deposited by reactive sputtering[13], while NiO was deposited by PLD[11]); therefore correlation between iDMI and the amount of NiO phase might be a universal relationship. This reveals that DMI can be tailored by tuning the quality of the NiO layer with respect to defects and/or the presence of Ni$_2$O$_3$ phase in the nickel oxide layer. Interestingly, the NiO phase is responsible for stronger iDMI favoring clockwise chirality if it is on the Co layer and anticlockwise chirality when Co is on top of the NiO layer. This might be quite surprising because it is the opposite of what was previously found for different systems (oxide/Co/Pt[21] and Pt/Co/oxide[21,28–30]). Considering that the iDMI originates from an exchange interaction between two neighboring FM spins coupled via a neighboring layer, we suppose that the additional contribution to iDMI comes from the interaction between Co and the antiferromagnetic NiO phase.

Conclusion

We have investigated the changes of the magnetic properties in the NiO/Co/Pt trilayer as a function of Co layer thickness. Magnetooptical studies reveal significant value of the magnetic anisotropy occurring in the PMA region and anticlockwise spin chirality within the Néel domain walls. BLS measurements confirm the presence of iDMI with a high value of $D_S = +2.0$ pJ/m. This value is higher than that of similar systems where the Co layer was in contact with NiO and systems where Co was in contact with other nonmagnetic oxides. The dependence between iDMI and the relative phase concentration of NIO shows that NiO is an additional source of DMI with a chirality that is opposite to that of other nonmagnetic oxides.

Methods

Samples with nominal structures Ti(4 nm)/Au(60 nm)/NiO(10 nm)/Co(0 ÷ 3 nm, wedge)/Pt(5 nm) were deposited on thermally oxidized silicon substrate using magnetron sputtering (Ti, Au, Pt and Co layers) or PLD (NiO layer) in a UHV multichamber system with base pressure below 2×10^{-8} mbar. The nominal thicknesses of the Ti, Au, Co, Pt, and NiO were calculated using deposition time and the deposition rate determined by X-ray reflectivity and/or profilometer measurements from calibration samples. The Co thickness was linearly varied along the sample with a slope of 0.15 nm/mm. This was realized using a moving shutter (slightly above the substrate) with constant velocity during deposition. For correct stoichiometry, the NiO layer was deposited in an oxygen-rich atmosphere ($p_O = 1.5 \times 10^{-5}$ mbar) in a separate UHV chamber[11]. After NiO deposition, the sample was transferred to magnetron sputtering chamber without breaking UHV conditions (during transfer, $p \leq 5 \times 10^{-8}$ mbar). This reduces oxidation of the Co layer, as discussed in our earlier work[8]. During deposition, the sample was kept in an external out-of-plane magnetic field $\mu_0 H_{dep} = -0.19$ T to increase EB coupling between Co layer and NiO layers. As the NiO layer is covered by the Co and Pt layers the evaluation of the NiO stoichiometry is not possible from direct XPS measurements. To verify the composition of the NiO layer the XPS measurements were performed on the 50 nm thick NiO deposited onto Si substrate in the same condition as for the full layer stack. The results are presented in the Supplementary Materials (Fig. S2).

PMOKE magnetometry measurements were performed using a laser beam with wavelength 635 nm focused on 0.3 mm spot at nearly normal light incidence.

A PMOKE microscope equipped with a CCD camera and an appropriate digital image processing software (in PMOKE configuration the measured signal intensity is proportional to the out-of-plane magnetization component) were used to: (i) record large field of view image of remanent magnetization distributions after out-of-plane saturation; (ii) determine local magnetization loops in the whole sample area with 10 μm lateral resolution. Asymmetric domain propagation was measured using PMOKE microscope with a pulsed magnetic field applied with simultaneous out-of-plane and in-plane components. All recorded PMOKE images were presented as differential images that were obtained after, pixel-by-pixel, gray scale intensity subtraction of the reference image obtained in initial state (with small bubble domain).

BLS experiments were performed in the backscattering configuration, illuminating the sample with p-polarized laser beam with a wavelength $\lambda = 532$ nm and beam spot size about 20 μm at variable incident angle Θ. In this geometry, the value of excited (absorbed) in-plane magnon wave vector k is equal to $4\pi/\lambda \sin\Theta$. The laser power was less than 70 mW to avoid sample overheating. The scattered light was collected by a focusing lens and its spectrum was analyzed by a Sandercock-type multi-pass tandem Fabry–Perot TFP-2 HC interferometer. The external magnetic field H_y was applied in the sample plane and normal to the scattering plane of the laser light. More detailed description of used BLS measurements is given in[31].

All measurements were performed at RT.

Data availability

All results presented in this paper are available from the corresponding author on reasonable request.

References

1. Gaurav Rana, K. et al. Room-temperature Skyrmions at zero field in exchange-biased ultrathin films. Phys. Rev. Appl. **13**, 044079. https://doi.org/10.1103/PhysRevApplied.13.044079 (2020).
2. Yang, H., Boulle, O., Cros, V., Fert, A. & Chshiev, M. Controlling Dzyaloshinskii–Moriya interaction via chirality dependent atomic-layer stacking insulator capping and electric field. Sci. Rep. **8**, 12356. https://doi.org/10.1038/s41598-018-30063-y (2018).
3. Lin, W. et al. Perpendicular magnetic anisotropy and Dzyaloshinskii–Moriya interaction at an oxide/ferromagnetic metal interface. Phys. Rev. Lett. **124**, 217202. https://doi.org/10.1103/PhysRevLett.124.217202 (2020).
4. Nembach, H. T., Jué, E., Evarts, E. R. & Shaw, J. M. Correlation between Dzyaloshinskii–Moriya interaction and orbital angular momentum at an oxide-ferromagnet interface. Phys. Rev. B. **101**, 020409(R). https://doi.org/10.1103/PhysRevB.101.020409 (2020).
5. Chen, R. et al. Large Dzyaloshinskii–Moriya interaction and room-temperature nanoscale skyrmions in CoFeB/MgO heterostructures. Cell Rep. Phys. Sci. **2**, 100618. https://doi.org/10.1016/j.xcrp.2021.100618 (2021).
6. Koplak, O. et al. Dzyaloshinskii-Moriya interaction determined from spin wave nonreciprocity and magnetic bubble asymmetry in Pt/Co/Ir/Co/Pt synthetic ferrimagnets. J. Phys. Condens. Matter. **34**, 85803. https://doi.org/10.1088/1361-648X/ac3c0a (2022).
7. Zhang, B. H., Hou, Y. S., Wang, Z. & Wu, R. Q. Tuning Dzyaloshinskii–Moriya interactions in magnetic bilayers with a ferroelectric substrate. Phys. Rev. B. **103**, 054417. https://doi.org/10.1103/PhysRevB.103.054417 (2021).
8. Kowacz, M., Anastaziak, B., Schmidt, M., Stobiecki, F. & Kuświk, P. Strong interfacial perpendicular magnetic anisotropy in exchange-biased NiO/Co/Au and NiO/Co/NiO layered systems. Materials **14**(5), 1237. https://doi.org/10.3390/ma14051237 (2021).
9. Walls, B. et al. Nanodomain structure of single crystalline nickel oxide. Sci. Rep. **11**, 3496. https://doi.org/10.1038/s41598-021-82070-1 (2021).
10. Uhlenbrockt, S., Scharfschwerdtt, C., Neumannt, M., Illing, G. & Freund, H.-J. The influence of defects on the Ni 2p and O 1s XPS of NiO. J. Phys. Condens. Matter **4**, 7973. https://doi.org/10.1088/0953-8984/4/40/009 (1992).
11. Kuświk, P. et al. Asymmetric domain wall propagation caused by interfacial Dzyaloshinskii–Moriya interaction in exchange biased Au/Co/NiO layered system. Phys. Rev. B. **97**, 024404. https://doi.org/10.1103/PhysRevB.97.024404 (2018).
12. Kuświk, P., Matczak, M., Kowacz, M., Lisiecki, F. & Stobiecki, F. Determination of the Dzyaloshinskii–Moriya interaction in exchange biased Au/Co/NiO systems. J. Magn. Magn. Mater. **472**, 29. https://doi.org/10.1016/j.jmmm.2018.10.002 (2019).
13. Kolesnikov, A. G. et al. Magnetic properties and the interfacial Dzyaloshinskii–Moriya interaction in exchange biased Pt/Co/NixOy films. Appl. Surf. Sci. **543**, 148720. https://doi.org/10.1016/j.apsusc.2020.148720 (2021).
14. Dhiman, A. K. et al. Thickness dependence of interfacial Dzyaloshinskii–Moriya interaction, magnetic anisotropy and spin waves damping in Pt/Co/Ir and Ir/Co/Pt trilayers. J. Magn. Magn. Mater. **519**, 167485. https://doi.org/10.1016/j.jmmm.2020.167485 (2021).
15. Dhiman, A. K. et al. Magnetization processes and magnetic domain structures in Ta/CoFeB/MgO stacks. J. Magn. Mag. Mat. **529**, 167699. https://doi.org/10.1016/j.jmmm.2020.167699 (2021).

16. Mazalski, P. *et al.* Ultrathin Co films with Pt and Au covers—magnetic and structural properties driven by Ga+ ion irradiation. *New J. Phys.* **23**, 023015. https://doi.org/10.1088/1367-2630/abde6d (2021).
17. Kootte, A., Haas, C. & de Groot, R. A. The electronic structure of ordered binary Co-Pt compounds. *J. Phys. Condens. Matter.* **3**, 1133. https://doi.org/10.1088/0953-8984/3/9/009 (1991).
18. Manchone, A. *et al.* X-ray analysis of the magnetic influence of oxygen in Pt/Co/AlOx trilayers. *J. Appl. Phys.* **103**, 07A912. https://doi.org/10.1063/1.2829896 (2008).
19. Kuświk, P. *et al.* Enhancement of perpendicular magnetic anisotropy of Co layer in exchange-biased Au/Co/NiO/Au polycrystalline system. *J. Appl. Phys.* **119**, 215307. https://doi.org/10.1063/1.4952706 (2016).
20. Mazalski, P. *et al.* Demagnetization of an ultrathin Co/NiO bilayer with creation of submicrometer domains controlled by temperature-induced changes of magnetic anisotropy. *J. Magn. Magn. Mater.* **508**, 166871. https://doi.org/10.1016/j.jmmm.2020.166871 (2020).
21. Kim, N.-H. *et al.* Improvement of the interfacial Dzyaloshinskii–Moriya interaction by introducing a Ta buffer layer. *Appl. Phys. Lett.* **107**, 142408. https://doi.org/10.1063/1.4932550 (2015).
22. Kim, N.-H. *et al.* Interfacial Dzyaloshinskii–Moriya interaction, surface anisotropy energy, and spin pumping at spin orbit coupled Ir/Co interface. *Appl. Phys. Lett.* **108**, 142406. https://doi.org/10.1063/1.4945685 (2016).
23. Hrabec, A. *et al.* Measuring and tailoring the Dzyaloshinskii–Moriya interaction in perpendicularly magnetized thin films. *Phys. Rev. B* **90**, 020402(R). https://doi.org/10.1103/PhysRevB.90.020402 (2014).
24. Han, D.-S. *et al.* Asymmetric hysteresis for probing Dzyaloshinskii–Moriya interaction. *Nano Lett.* **16**, 4438. https://doi.org/10.1021/acs.nanolett.6b01593 (2016).
25. Di, K. *et al.* Direct observation of the Dzyaloshinskii–Moriya interaction in a Pt/Co/Ni Film. *Phys. Rev. Lett.* **114**, 047201. https://doi.org/10.1103/PhysRevLett.114.047201 (2015).
26. Kostylev, M. Interface boundary conditions for dynamic magnetization and spin wave dynamics in a ferromagnetic layer with the interface Dzyaloshinskii–Moriya interaction. *J. Appl. Phys.* **115**, 233902. https://doi.org/10.1063/1.4883181 (2014).
27. Moon, J.-H. *et al.* Spin-wave propagation in the presence of interfacial Dzyaloshinskii–Moriya interaction. *Phys. Rev. B* **88**, 184404. https://doi.org/10.1103/PhysRevB.88.184404 (2013).
28. Belmeguenai, M. *et al.* Interfacial Dzyaloshinskii-Moriya interaction in perpendicularly magnetized Pt/Co/AlOx ultrathin films measured by Brillouin light spectroscopy. *Phys. Rev. B* **91**, 180405(R). https://doi.org/10.1103/PhysRevB.91.180405 (2015).
29. Boulle, O. *et al.* Room-temperature chiral magnetic skyrmions in ultrathin magnetic nanostructures. *Nat. Nanotech.* **11**, 449. https://doi.org/10.1038/NNANO.2015.315 (2016).
30. Cho, J. *et al.* Thickness dependence of the interfacial Dzyaloshinskii–Moriya interaction in inversion symmetry broken systems. *Nat. Commun.* **6**, 7635. https://doi.org/10.1038/ncomms8635 (2015).
31. Kurant, Z. *et al.* Magnetic ordering in epitaxial ultrathin Pt/W/Co/Pt layers. *J. Magn. Magn. Mater.* **558**, 169485. https://doi.org/10.1016/j.jmmm.2022.169485 (2022).

Acknowledgements

Author contributions

P.K. and A.M. designed the study. M.K., B.A. and M.M. sample deposition and characterization supervised by P.K. U.G., A.K.D. and R.G. performed BLS measurements and data analysis. P.M., M.K., and I.S. performed magnetooptical studies and data analysis. E.M. performed XPS measurements and data analysis. M.K. and P.K. contributed to the interpretation of the results. P.M., P.K. and A.M. planned the idea of the experiments. P.M., I.S, P.K. and R.G. wrote the manuscript in consultation with all authors.

Competing interests

The authors declare no competing interests.

Additional information

Supplementary Information The online version contains supplementary material available at https://doi.org/10.1038/s41598-022-16997-4.

Correspondence and requests for materials should be addressed to P.M. or P.K.

Reprints and permissions information is available at www.nature.com/reprints.

Publisher's note Springer Nature remains neutral with regard to jurisdictional claims in published maps and institutional affiliations.